CHARACTERIZATION OF 3D PRINTED CONDUCTIVE SOFT ROBOTIC ELEMENTS

OZAN ARSLAN

EYLÜL 2022

ÇANKAYA UNIVERSITY

GRADUATE SCHOOL OF NATURAL AND APPLIED SCIENCES

DEPARTMENT OF MECHANICAL ENGINEERING
MASTER'S THESIS IN
MECHANICAL ENGINEERING

CHARACTERIZATION OF 3D PRINTED CONDUCTIVE SOFT ROBOTIC ELEMENTS

OZAN ARSLAN

EYLÜL 2022

ABSTRACT

CHARACTERIZATION OF 3D PRINTED CONDUCTIVE SOFT ROBOTIC ELEMENTS

ARSLAN, Ozan

Master of Science in Mechanical Engineering

Supervisor: Asst. Prof. Dr. Özgün SELVİ

September 2022, 52 Pages

The thesis makes the characterization of 3D printed conductive soft robotic elements by using data to develop an evaluation model from specific to general.

In the first step, the thesis provides the findings of past research and related articles as a literature survey. The chapter begins with the fundamentals and importance of 3D printing and continues with an explanation of the ability of soft robotic 3D printing. Examples from soft robotic works follow the previous chapter, and sensing at soft robotic elements is briefly explained as the next step. Finally, the section ends with related topics and focuses on other conductive soft robotic element articles. The last part explains the aim of the research and its motivation.

The following chapter emphasizes methods and material selection topics thoroughly. The next section presents the used parameters and detailed information about the physical boundaries of the material. The sequent section provides information about printing constants and machine setup. The final part informs about curing time, molding phases, and molding setup.

The third chapter starts with a detailed explanation of test setup and expresses every step of test setup assembling, including two different test molds and specimen holders. The chapter continues with the testing process and shows every single setup parameter for providing data for future research. The last part of the chapter focuses

on the test result and discusses test results through graphs made using test result data. Final generalizations are given in this section.

The final chapter finishes the article by giving a conclusion to all work. The following sections tell about future work and possible usage suggestions.

The appendices have pictures of test results as tables from both tests.

Keywords: Soft Robotics, Characterization, Conductive, 3D Printed

ÖZ

3 BOYUTLU BASILAN İLETKEN YUMUŞAK ROBOTİK ELEMANLARININ KARAKTERİZASYONU

ARSLAN, Ozan

Makine Mühendisliği Yüksek Lisans

Danışman: Dr. Öğr. Üy. Özgün SELVİ

Eylül 2022, 52 sayfa

Tez, özelden genele doğru bir değerlendirme modeli geliştirmek için verileri kullanarak 3D baskılı iletken yumuşak robotik elemanların karakterizasyonunu yapar.

İlk adımda, tez, literatür taraması olarak geçmiş araştırmaların ve ilgili makalelerin bulgularını sunar. Bu bölüm, 3D baskının temelleri ve önemi ile başlar ve yumuşak robotik 3D baskı yeteneğinin açıklaması ile devam eder. Yumuşak robotik çalışmalardan örnekler ve yumuşak robotik elemanlarda algılama kısaca açıklanır. Son olarak, bölüm ilgili araştırmalarla sona erer ve diğer iletken yumuşak robotik eleman makalelerine odaklanır.

Takip eden bölümün ilk kısmı, yöntemleri ve malzeme seçimi konularını kapsamlı bir şekilde vurgulamaktadır. Bir sonraki kısım, kullanılan parametreleri ve malzemenin fiziksel sınırları hakkında ayrıntılı bilgileri sunar. Üçüncü kısım, yazdırma sabitleri ve makine kurulumu hakkında bilgi sağlar. Son kısım, kürleme süresi, kalıplama aşamaları ve kalıplama kurulumu hakkında bilgi verir.

Üçüncü bölüm, test kurulumunun ayrıntılı bir açıklamasıyla başlar ve iki farklı test kalıbı ve numune tutucu da dâhil olmak üzere test kurulumunun her adımını açıklar. Bölüm, test süreciyle devam eder ve gelecekteki araştırmalar için veri sağlamak adına kurulum parametrelerini gösterir. Bölümün son kısmı, test sonucuna odaklanır ve sonuçları kullanarak oluşturulan grafikler aracılığıyla sonuçları tartışır.

Son bölüm, çalışmaları karara bağlayarak makaleyi tamamlar. Kalan kısımlar gelecekteki çalışmalar ve olası kullanım önerileri hakkında öneriler vermektedir.

Ekler kısmı bulunan sonuçların tablo halinde sunulduğu bir fotoğraf içermektedir.

Anahtar Kelimeler: Yumuşak Robotlar, Karakterizasyon, İletken, 3 Boyutlu İmalat

ACKNOWLEDGEMENT

I would like to express my sincere gratitude to my parents and my wife for their support and sacrifice for me. I want to thank to my mental advisor and supporter, Onat TOTUK, for always giving support to me. Besides, I would like to thank İbrahim EKİCİ for being a supportive friend. Finally, I want to express my gratitude to Arven; her memories will ever shine in my mind.

Special thanks to my supervisor Asst. Prof. Dr. Özgün SELVİ for the excellent guidance and for providing me with an excellent atmosphere to conduct this research. My special gratitude also goes to the rest of the thesis committee for the encouragement and insightful comments.

TABLE OF CONTENTS

LIST OF TABLES

LIST OF FIGURES

LIST OF SYMBOLS AND ABBREVIATIONS

SYMBOLS

cm	: Centimeter
m	: Meter
in	: Inches
g	: Grams
sec	: Seconds
min	: Minutes
kn	: Kilonewton
MPa	: Megapascal
m3	: Cubic Meter
cc	: Cubic Centimeter
cps	: Centipoise
°C	: Centigrade
°F	: Fahrenheit

ABBREVIATIONS

MIS	: Minimally Invasive Surgery
TPU	: Thermoplastic Polyurethane

CHAPTER I

INTRODUCTION

3D printing is one of the most rapidly evolving and popular science areas. Fused Deposition Modelling (FDM) is one of the seven methods of Additive Manufacturing that may be used to create Computer-Aided Designed (CAD) objects by layering melted plastics. Many different pieces can be printed using 3D printing from novel materials to achieve freedom on softness and other material properties [1–3].

The term soft material can be explained as material that is highly capable of deformability [4]. As FDM can be used in producing these materials, the molding method also can be used. Plastic make-up silicone, also known as "Dragon Skin," is the best-known material for the molding of soft materials. Soft materials are used in the production of soft sensors and tissue engineering [5, 6]. Softness provides elasticity, bending, and buckling capacity to sensors without taking internal damage.

Conductibility is the major point of soft sensors. So, conductive soft filaments were used for producing soft sensors. This provided obtaining electrical data from soft robotic parts and obtained data were used in the characterization of soft sensors.

The bending and tensile tests are two basic tests for understanding the elasticity versus conductibility profile of soft sensors. Results can be listed in the type of elongation percentage, and this will be a source of approximation for maximum elongation without taking damage. A similar approach also provides results of the same stripe for the bending test.

The aim of this thesis is using conductive filament on the soft sensors as a result of a lack of studies on that specific area. There is no characterization and prevailing data about the mixed usage of soft material and conductive flexible filaments on soft sensors. The study was planned to yield soft robotic fingers, which are very popular in soft robotics, and other technologies as future work [7].

1

1.1 LITERATURE SURVEY

3D printing is one of the most important topics in the scientific area [8–12]. The procedure provides complex shape production with low effort. Freedom of complexity becomes the impulsion of both industrial design and scientific design. Scientific test specimens or connection and measurement tools can be produced easier with 3D printing rather than conventional production methods. The method uses plastic particles or powders as raw material. The heating probe, also called an extruder, melts raw plastic and places it on the printing bed by following a production route like CNC routing machines. Extrusion is supported by a servomotor for continuous production. Product is created layer by layer, and all parameters like layer thickness or layer count can be set manually. Thanks to this customizability, various shapes, and material mixtures can produce with 3D printing.

3D printing of soft robotic elements is a trending branch of the 3D printing area [13–15]. Technological developments cleared the path for scientists, so producing soft robotic components with low-cost customer-type 3D printers is became within the bounds of possibility. That opportunity was examined by Selvi Ö et al. in the "3D Printing Soft Robots Using Low-Cost Consumer 3D Printers" article [16]. The article proves the ability to produce shore A65 soft robotic elements by showing test and analysis results as proof. Fundamental principles of soft material printing and possible shapes are also discussed in the article. T.J Wallin et al. mentioned the basics and benefits of 3D printing for producing complex shapes such as soft robotics elements [17]. Different 3D printing types were examined, new technologies were discussed, and future usage areas were mentioned about soft robotics.

Yee Ling Yap et al. reviewed 3D printing processes and materials of soft robotic elements [18]. The advantages and disadvantages of different techniques were discussed, and typical geometries of different production methods were explained. Shape memory polymers were emphasized as one of the most exciting and trending materials. 3D printing was referred to as the future of soft robotic production. Foam is another trending material in soft robotic production. Luca Somm et al. mentioned the fabrication method of foam-based soft robotic elements with embedded sensing [19]. Softness and cheapness of the material were highlighted, and possible usage areas for soft foam-based embedded sensing soft robotic elements were explained.

Like production material, inner structure and infill can also change according to design [20, 21]. Fluid strengthening of soft robotic elements can be an example of different infill types. Usually, air fills the voids of soft robotic elements in general applications, but specific studies tried to infill and strengthen soft robotic elements with fluids like water. "Strengthening Effect of Flooding in 3D Printed Porous Soft Robotics Scaffolds" article, written by Selvi Ö. et al. one of the best sample cases on different infill studies [22]. The authors present gyroid infill-shaped specimens and show the strengthening effect of fluid, which uses infill voids to strengthen the structure.

Fluid-driven soft elements can be produced with internal sensing too. Internal sensing brings safety to human-robot interaction and interoperation through flexibility and deformability. Polygerinos et al. reviewed the fluid-driven soft robotic elements and their application in human-robot interaction [23]. Authors primarily focused on intrinsically soft, elastomeric robots that work with fluidic pressurization power. The human-robot interface uses soft robots or their elements as actuators, sensors, or control members for different applications. Gorissen et al. exemplify the use of soft robotics elements as actuators [24]. The article also mentions particular soft actuator design and their production processes. Runciman M. et al. explain the usage of soft robotic actuators in minimally invasive surgery [25]. Minimally invasive type surgeries are made with deformable surgical instruments, and soft robotic elements and actuators should have required deformability. The article highlights the usage areas and importance of soft robotic elements in MIS. Using flexibility for executing motions like threading through a needle is the achievement of scientists who observed the nature of developing new technologies.

Observing and copying nature is called biomimetics in the science world [26, 27]. Bioinspiration is treated in the "Bio-inspired soft robotics: Material selection, actuation, and design" article by Stephen Coyle et al. [28]. The article additionally touched on material selection, actuation, and design steps of bioinspired soft robotic designs. Besides, biomimetics develops human-robot interactions by showing new and effective ways for robotic arms. Scientist like C. Laschi et al. bioinspired from octopus to develop a robotic arm that can elongate and holds amorphous objects [29]. The tentacle arm can deform due to lacking joint and rigid link so, which provides limitless freedom of movement.

Adding conductance is a way of enhancing the usage area of soft robotic parts. Conductive filament brings embedded electronic opportunities to part, and thanks to the gained opportunities, soft sensors and actuators can be produced easier [30–32]. Conductive filaments are scrutinized in the "Electrically conductive filament for 3D-printed circuits and sensors" by Sen Wai Kwok et al. article [33]. Scientists tried to fabricate, characterize, make stress tests, and application of 3D-printed conductive elements. A low-cost thermo-plastic conductive composite was used for the research project. This kind of thermo-plastics has been acquired by embrue carbon particles to the filament. Test specimens were produced in different shapes from ABS and conductive composite for the research. The conductive layer was used as a sensor mechanism and tried different types of sensors, such as temperature and sunlight. Results showed the success of 3D-printed conductive sensors. Some of the result graphs from the article are given below as Figure 1.1.
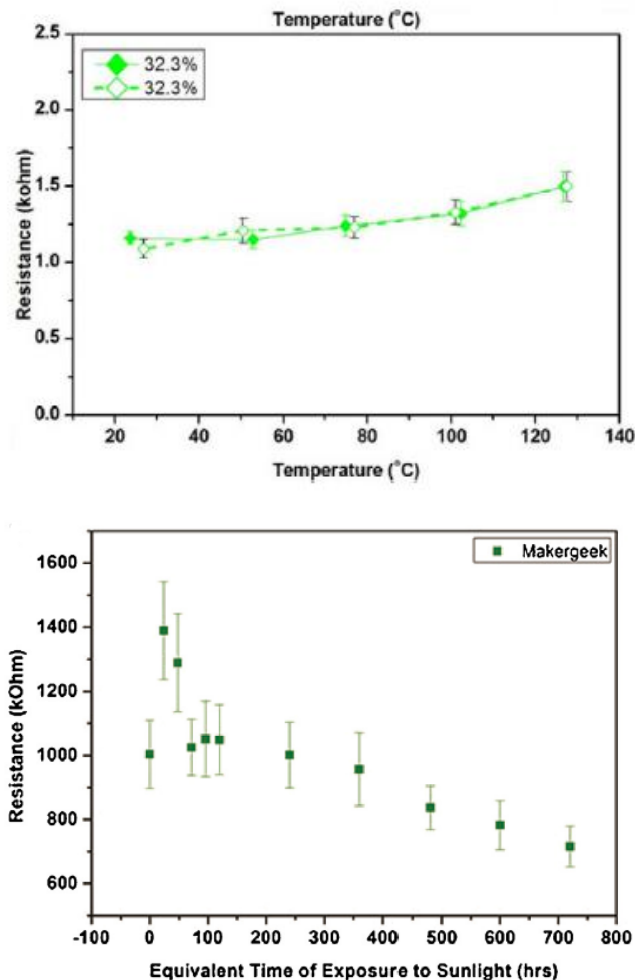

Figure 1.1: Example Result Graphs from Ref. [33].

Alexander M. Hart presented a thesis on a specialized category of soft sensors that is named as "Positional Estimation of Soft Actuators through Embedded Sensing."[34] The article aimed to combine sensors with soft robotic elements like actuators. Embedded sensing was used as a sensor for estimating the position of the soft actuator. The study also showed that unpredictable motions of soft robotic elements could be avoided by sensing the motion on the fly.

1.2 MOTIVATION

Conductive soft 3D filaments are one of the new trends in the soft robotic area. Scientific researches and production tests continue to develop new technologies and usage areas. Paving the way for future studies is the key to accelerating the development of new technologies like wearable technology.

Characterization of the filaments is one of the best options for easing future research studies. Although there are characterization studies for soft robotics elements, the characterization of conductive soft robotic elements was not made [35, 36]. The output of this study can be the starting point of the next theses, and the conductive soft robotic production branch can enhance.

Finally, the data and output of the experiment could be the master thesis, and articles could be produced from the thesis.

1.3 AIM

Paving the way for future research by characterizing the material in different shapes and different loads is the main target of this study.

Trying the production of different shapes and showing the shape effect on sensor resistance difference is aimed at this study. Finding optimal configurations for production is the benefit of this aim. Gathered configuration data were shared in Table 2.4 in the methods chapter with all units.

Moreover, the study tries to specify future work and future usage areas. Wearable technology was specified as one of these areas.

CHAPTER II

MATERIALS & METHODS

2.1 MATERIAL SELECTION

3D printers are the best way of producing complex shapes [37]. Due to the complexity of the conductive middle layer shape, it was produced with a 3D printer. EEL filament of NinjaTek brand was selected as the conductive material. Filament contains carbon particles for being able to conduct electricity. General, mechanical, and conductive property data were provided by NinjaTek Company's datasheet. In addition, test specifications were indicated by the company in the same datasheet. The table of information that is obtained from the data-sheet is given below as Table 2.1.

Table 2.1: Technical and Physical Properties of EEL Filament.

General Properties	Test Method	Imperial
Specific Gravity	ISO 2781	1.18 g/cm^3
Mechanical Properties	**Test Method**	**Metric**
Tensile Strength	ISO 527-2/51/500	12 MPa
Tensile Elongation	ISO 527-2/51/500	355%
Tensile Stress at:		
50% Elongation	ISO 527-2/51/500	8 MPa
100% Elongation	ISO 527-2/51/500	9 MPa
300% Elongation	ISO 527-2/51/500	11 MPa
Tear Strength Nicked	ISO 34-1B	84 kn/m
Hardness	ISO 868	90A
Conductive Properties	**Test Method**	**Metric**
Volume Resistance	ANSI/ESD STM 11.12	1.5 x 10^3 ohm
Surface Resistance	ANSI/ESD STM 11.11	1.5 x 10^3 ohm
Shore Hardness	90A	

The conductive filament is made by a mixture of elastic filament base and carbon powder. Carbon powder is the source of conductibility. As an elastic filament base, TPU plastic particles are used. Thus, the shore value of the conductive filament is equal to the TPU filament. Due to the lack of abilities of the department, the

conductive flexible filament was bought from commercial ones instead of producing. The chosen filament is EEL by NinjaTek brand.

The silicone layer composes of a curing chemical and silicone base mixture. The mixture is also called "Dragon Skin" and comes as transparent. Silicone mixture technical data was tabled by information that was taken from the manufacturer and given as Table 2.2 below.

Table 2.2: Technical Properties of Dragon Skin.

Specific Mass	1,07 g/cc
Specific Volume	1,61 m3/kg (25,8 cu. in/lb.)
Decay Time	4 Minutes
Curing Time	30 Minutes
Shore Hardness	10A
Tensile Strength	32,75 Bar (475 psi)
% 100 Module	1,51 Bar (22 psi)
Elongation at Break	1.000%
Shrinkage Allowance	<0,001 in/in
Mixture Ratio in Volume	1:1
Mixture Ratio in Mass	1:1
Color	Transparent
Min Temperature	-53 °C (-65 °F)
Max Temperature	252 °C (450 °F)
Mixture Viscosity	23.000 cps

2.2 METHODS

In this section, selected processes and programs were indicated. Explanations were given with examples and supportive pictures.

The experiment was conducted in two phases. The first phase is preparing conductive parts by using a 3D printer. The conductive filament was used for that phase. Soft silicon which is also known as dragon skin was used for preparing shells around the conductive layer. That shell is also the main body of the sensor. Also, production of the test apparatus was made on a 3D printer. The test apparatus was designed specifically for the experiment on a 3D design program. Previous scientific experience with 3D printers and soft robotics helped me on my way to finishing this master of science thesis.

Parameters were selected as averages of the recommended values at the beginning of the trial phase. Experience showed that the best quality could be achieved

with 222°C extruder temperature and 30°C bed temperature values. These values were set as nominal printing temperatures for providing the quality of test specimens. The specimens were designed and manufactured in two parts silicone layer and 3D-printed conductive layer. Recommended and used parameters were given in Table 2.3 and Table 2.4 below.

Table 2.3: Recommended Parameters for Printing.

Recommended Parameters for Printing	
Extruder Temperature	220°C - 230°C
Platform Temperature	Room temperature to 45°C
Print Speed	Top and bottom layers: 15-20 mm/sec (900-1800 mm/min)
	Infill speeds: 45-60 mm/sec (2700-3600 mm/min)

Table 2.4: Used Parameters for Printing.

Used Parameters for Printing	
Extruder Temperature	222°C
Platform Temperature	43°C
Print Speed	Top and bottom layers: 15 mm/sec (900 mm/min)
	Infill speeds: 50 mm/sec (3000 mm/min)
Infill Ratio	95%

Test specimen dimensions were set by paying attention to the observation and measurement area that remains after clamping from both sides of the specimen. Length and width were identified on nominal finger size according to the "The Measure of Man and Woman: Human Factors in Design" book of Tiley by considering the slenderness of the test specimen for observing elongation on tension [38]. Conductive measurement probes were added to the test specimen design owing to electrical measurements were planned to make by a multimeter. Different shapes were produced to examine the effect of conductive layer shape on resistance change. Pictures of designed conductive layers were given below from Figure 2.1 to Figure 2.5.
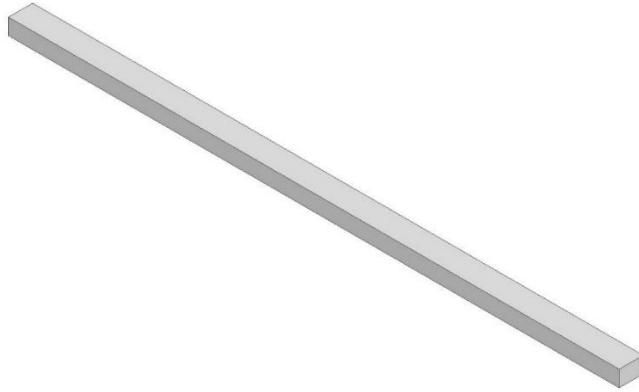
Figure 2.1: Picture of Straight Line Profile Design.
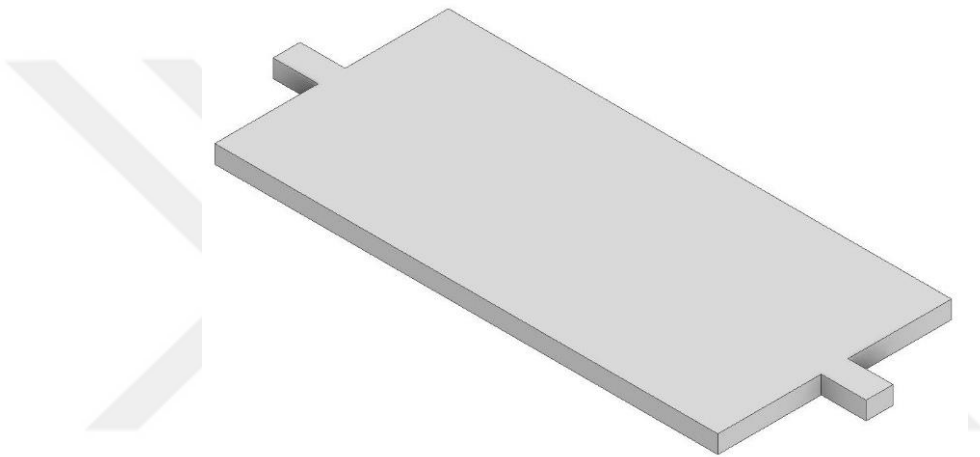
Figure 2.2: Picture of Rectangular Profile Design.

Figure 2.3: Picture of Honeycomb Profile Design.
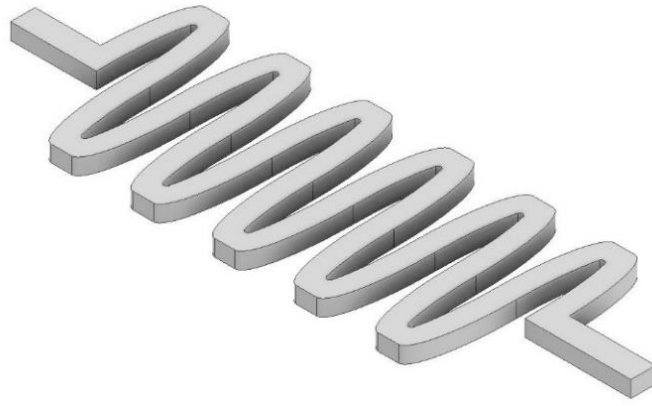
Figure 2.4: Picture of "S" Shaped Profile Design.
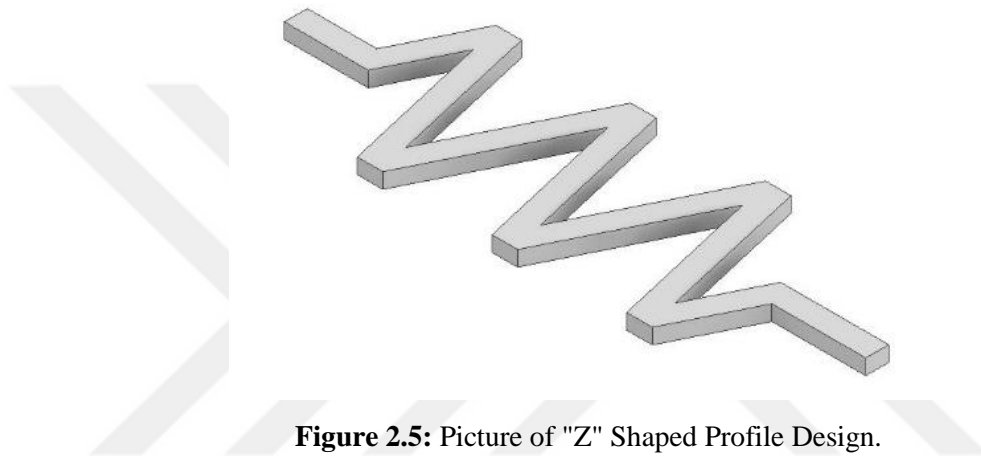
Figure 2.5: Picture of "Z" Shaped Profile Design.

The shape of the conductive layer was chosen from common shapes around the scientific area. Promising shapes were determined after preliminary tests and they were produced at 3 different thicknesses for detailed examination. Produced shapes were placed into pre-prepared undried dragon skin as the middle layer, and the top side was again filled with the dragon skin. The process was applied to obtain sandwich-like test specimens.
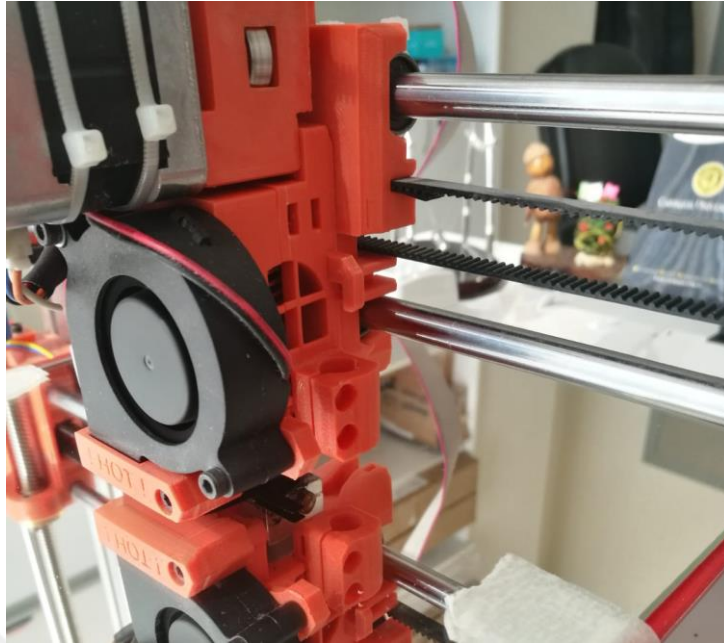
Figure 2.6: 3D Printing Phase of Rectangular Shape Conductive Layer.

Due to the suggested low bed temperature, lack of adhesion was one of the problems. The solution was found as that printing was made to the glass surface to increase the adhesion of extruded material. With increasing adhesion, easy reveling became a side benefit.
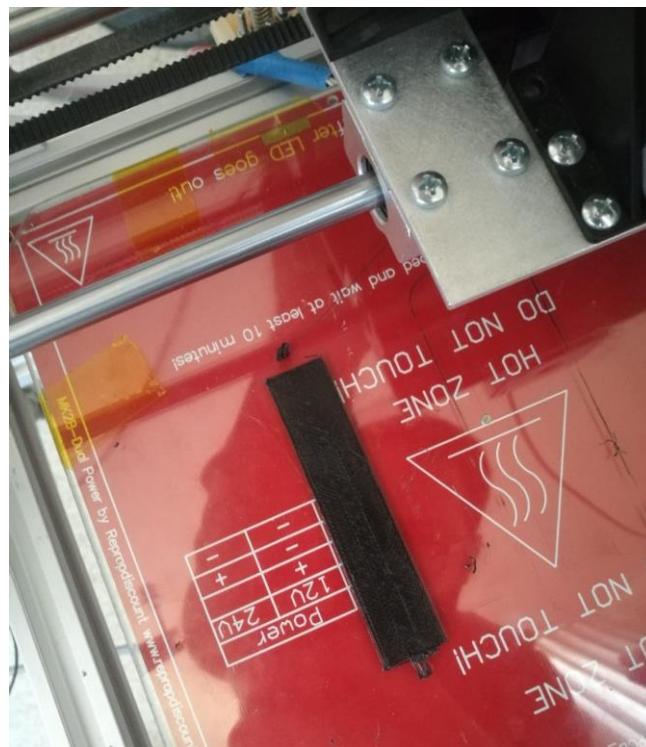
Figure 2.7: 3D Printed Rectangular Shaped Conductive Layer.

Photo block was used in the preparation of plastic casting molds due to its easily cuttable characteristic. The dimensions of the test specimen were transferred to the photo block thus cutting operation was handled and casting molds were produced. A silicone gun was used in the bonding process. Conductive probe holes were opened through the long side.

Dragon skin mixture came as two separate chemicals named "Cure A" and "Cure B." Two cures were mixed in a 50% - 50% ratio, as the manufacturer advised. As follows, the first layer of the test specimen was poured and 3D printed conductive layer was placed with no time due to avoid the freezing of silicone. In the final step, the second layer was poured. Molds were put on to freezing for 6 hours. Since separate molds were produced for every single part, the molds were cut carefully. Drying time was selected as 6 hours according to the output of trial and error experience. Pictures of printed parts in dried dragon skin coats were given below from Figure 2.8 to Figure 2.11.

Figure 2.8: Prepared Straight Line Shape Conductive Layer Test Specimens.
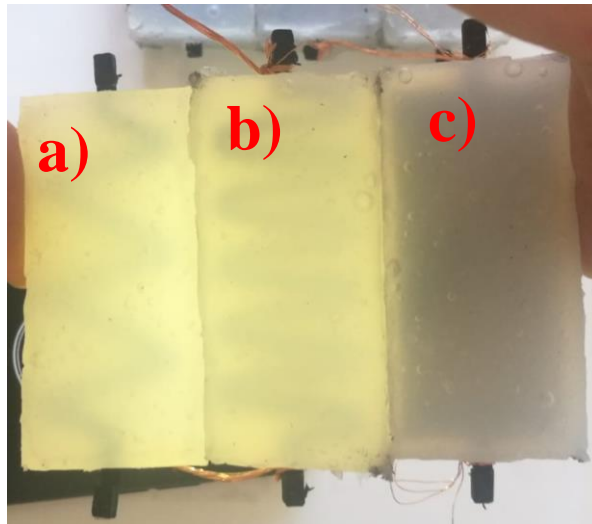
Figure 2.9: Prepared Test Specimens: a) "Z" Shaped Conductive Layer Test Specimen, b) "S" Shaped Conductive Layer Test Specimen, c) Rectangular Shaped Conductive Layer Test Specimen.
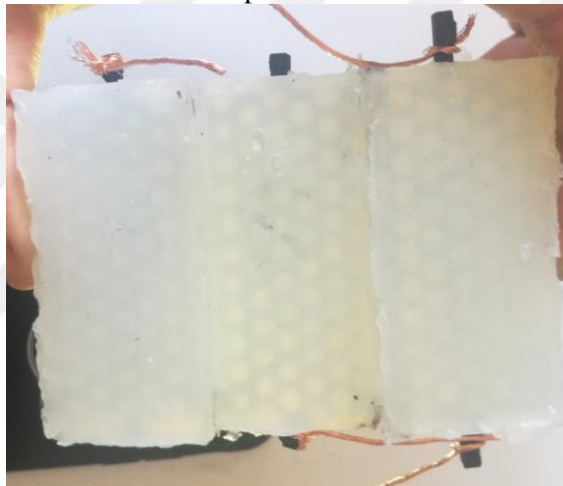
Figure 2.10: Prepared Honeycomb Shape Conductive Layer Test Specimens.
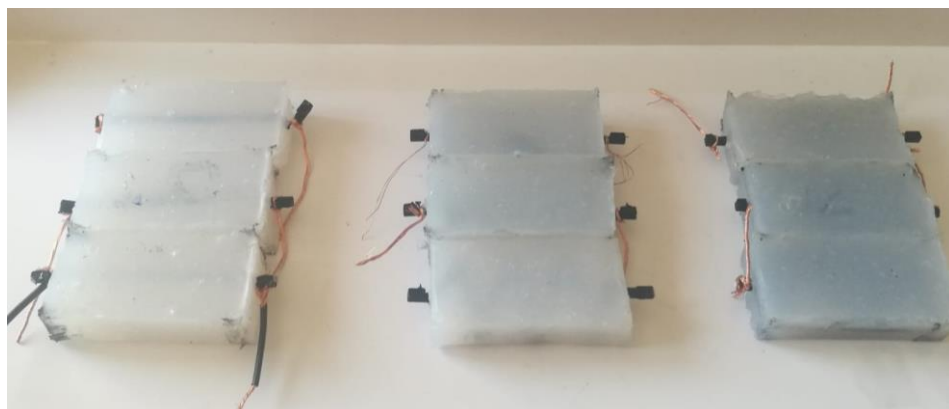
Figure 2.11: All of the Prepared Test Specimens.

CHAPTER III

TEST

3.1 TESTS

3.1.1 Preparing Test Setups

Tests are the foremost part of the research process inasmuch as characterization, all comments and inferences were made by using test data. Moreover, tests and results should be repeatable for providing scientificness of research. In line with this purpose, tests were standardized through mountable test setups, calibrated measurement tools, and using the same environmental conditions. Mountable test apparatus 3D was printed for the bending test. ABS was selected as test setup material. Different length, width, and height combinations were calculated and 30°, 45°, and 60° angles were provided. The bending test apparatus was designed in two parts to ease mounting and demounting. The upper part was planned in the semicircular shape and named as forcing part; the bottom part was planned on lunate and named as base part. Bending test setup images from different perspectives were given in Figure 3.1 and Figure 3.2 below.

Figure 3.1: Width Comparison of Bending Test Setup Apparatus.

Figure 3.2: Height Comparison of Bending Test Setup Apparatus.

Semicircular-shaped forcing apparatus designed at different sizes to provide required angles, and comparisons between the apparatus were given below in Figure 3.3.

Figure 3.3: Size Comparison of Bending Test Setup Forcing Apparatus.

Lunate-shaped base apparatus is designed at different sizes to provide required angles. Comparisons between the apparatus were given below in Figure 3.4.

Figure 3.4: Size Comparison of Bending Test Setup Base Apparatus.

The tensile test was made with a special test setup that is specially designed for the purpose. Brass was selected as the test setup material due to its easily processable nature. The setup was planned as three sections and five main parts. In the first section, the setup base was mounted to the pre-prepared white box to avoid visual complications. In the second section, the sliding jaw base was placed on the setup base and they were assembled by the bolt. Thanks to a 1 mm pitch distance, the M6 bolt was selected for providing controlled motion on a millimeter base. Finally, the last section, which is named demountable jaws, was placed on the sliding jaw by screwing. Base parts were designated as:

- Setup Base
- Left Sliding Jaw
- Right Sliding Jaw
- Left Demountable Jaw
- Right Demountable Jaw

Besides, a tape measure was mounted in front of the test setup to validate the movement amount. Assembled tensile test setup pictures were given in Figure 3.5 and Figure 3.6 below.
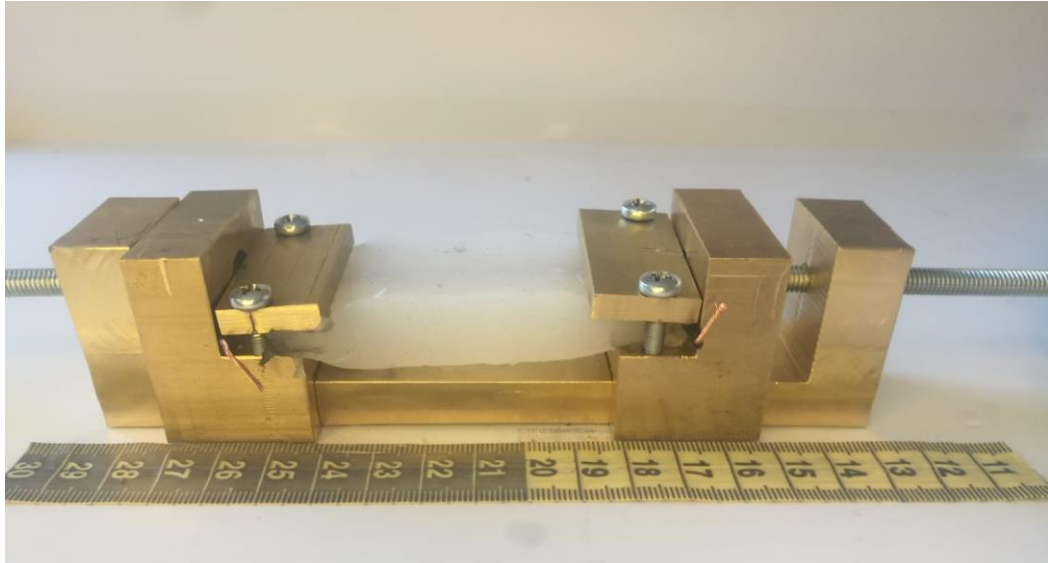
Figure 3.5: Assembled Tensile Test Setup Apparatus.
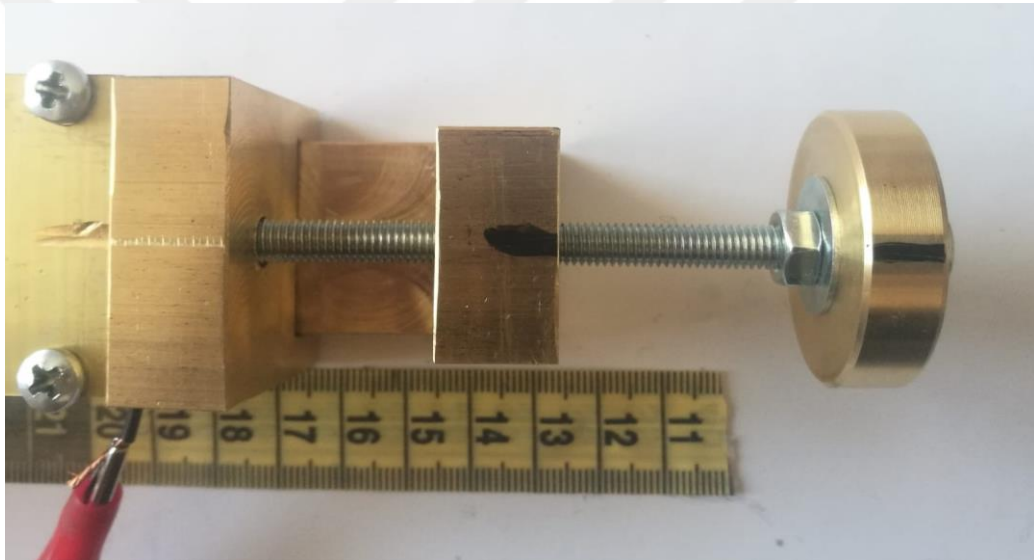
Figure 3.6: Upper View of Assembled Tensile Test Setup Apparatus.

3.1.2 Bending Test

Testing started right after the test setup preparation. A plastic latch clamp was used on the bending test to force the upper and bottom parts of the test apparatus towards each other. While the upper and bottom parts got close to each other, the bending angle of the test specimen got bigger. The constant pressing force was applied between different test specimens thanks to the constant force output of the plastic latch clamp. Selecting all the test components from plastic brought a big advantage which is the electrical insulation of the system. Pressed cases of test specimens between test apparatus were given from different angles of view below in Figure 3.7 and Figure 3.8.
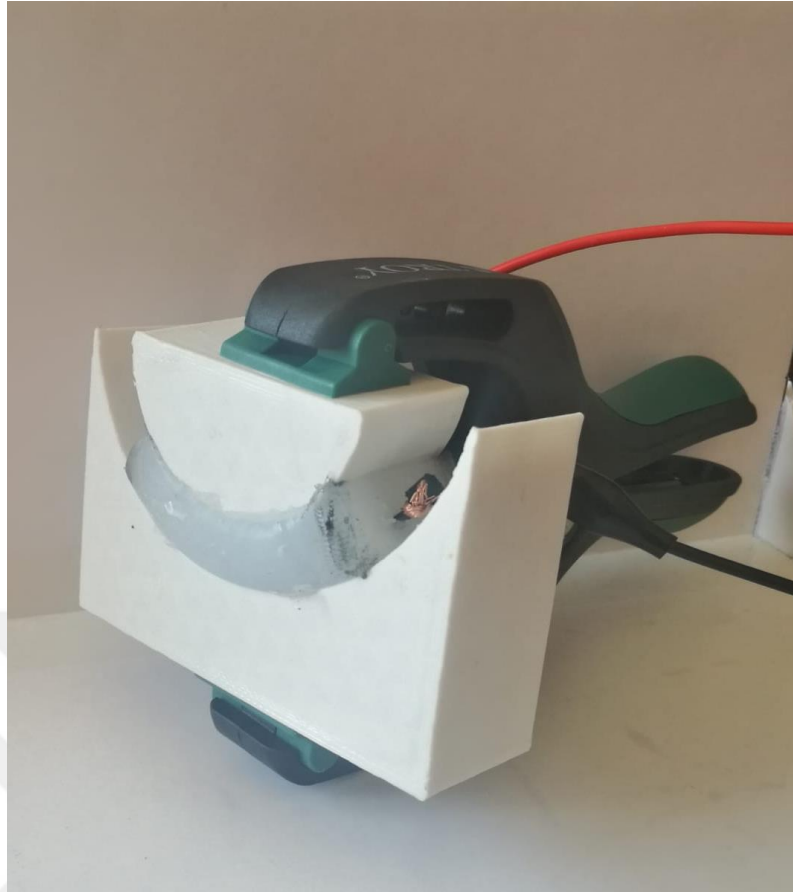
Figure 3.7: Test Specimen Placed and Clamped On Bending Test Setup.
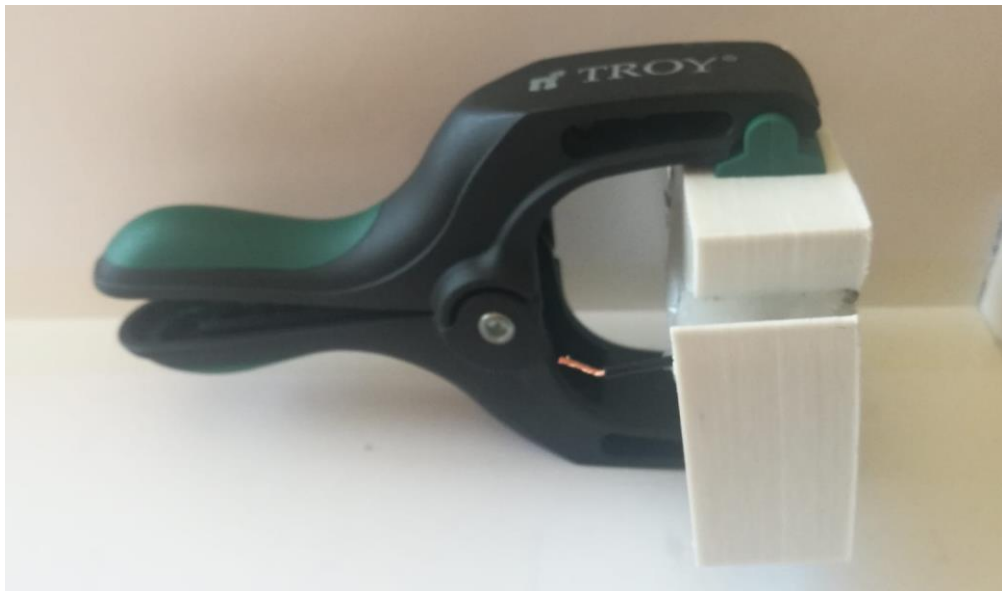
Figure 3.8: Test Specimen Placed and Clamped On Bending Test Setup from Different Angle of View.

3.1.3 Tensile Test

Digital Multimeter was used on both bending test measurements and tensile test measurements. Digitalizing the measurement tool avoided the observer error besides zero error avoided owing to using the calibrated tool. The measurement moment from the tensile test was presented in Figure 3.9 following.
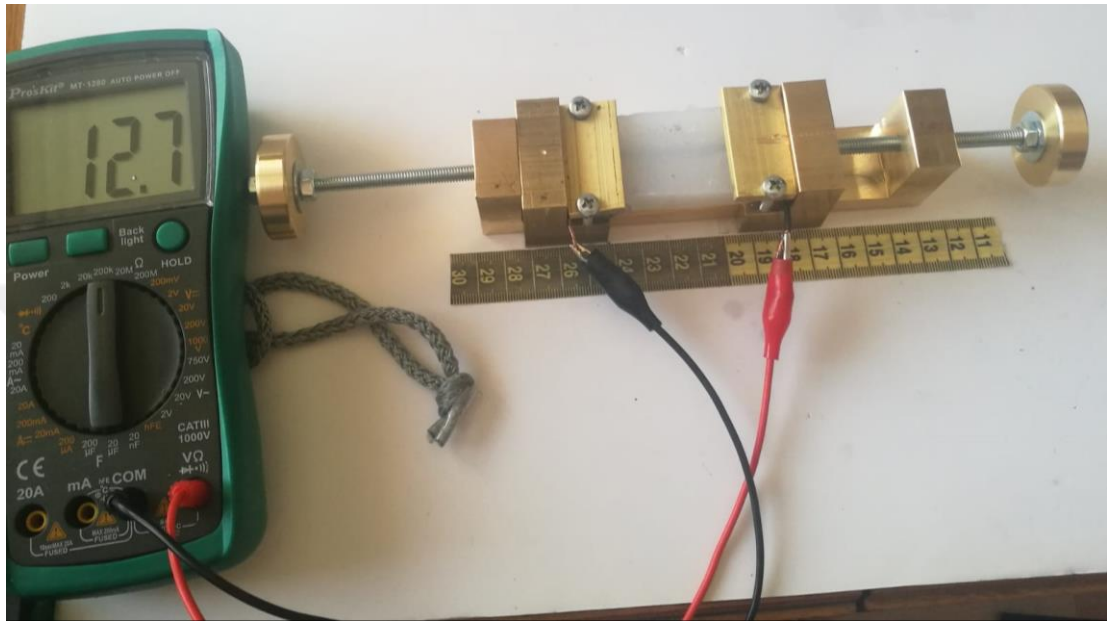
Figure 3.9: Measurement Moment from Tensile Test.

Tensile test was conducted by squeezing the test specimen between sliding demountable jaws and pinning by compress force of screws. The turning knob was marked for understanding the starting and finishing point of one turn. Since one turn equalized to 1 mm by choosing an M6 bolt, the test specimen was stretched one by one on a millimeter base. A tape measure is used to verify the movement amount and a double check was made thanks to that idea. The whole system can be seen in Figure 3.10 below.
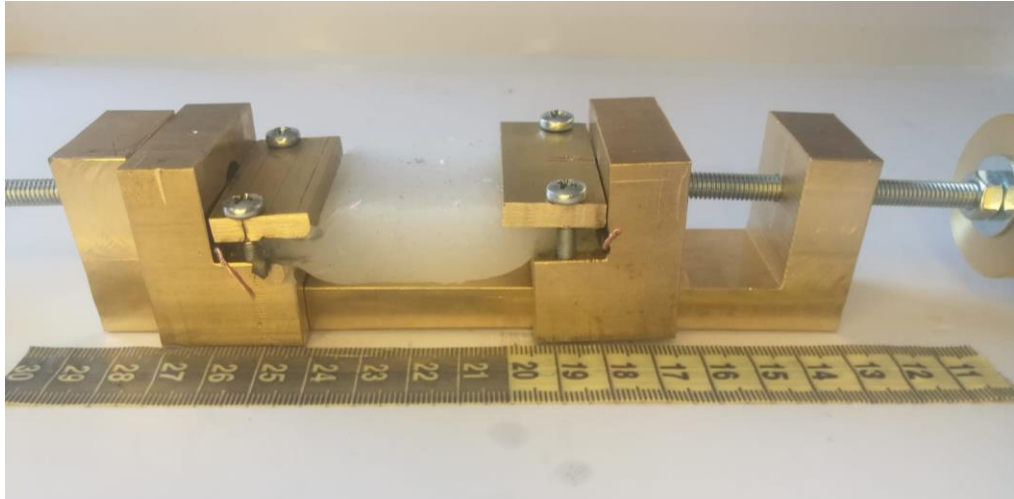
Figure 3.10: Test Specimen Placed and Clamped On Tensile Test Setup.

Insulation is a very critical point of the tensile test as in the bending test. Brass is not an insulating material so insulation was applied to the test setup. Hot silicone was used as insulation material and it was spread to the surface of jaws that contact with the test specimen surface. Digital multimeter probes were also metal but insulation worked for them as well. A picture that shows white box background and a digital multimeter from the resistance measurement moment were given below in Figure 3.11.
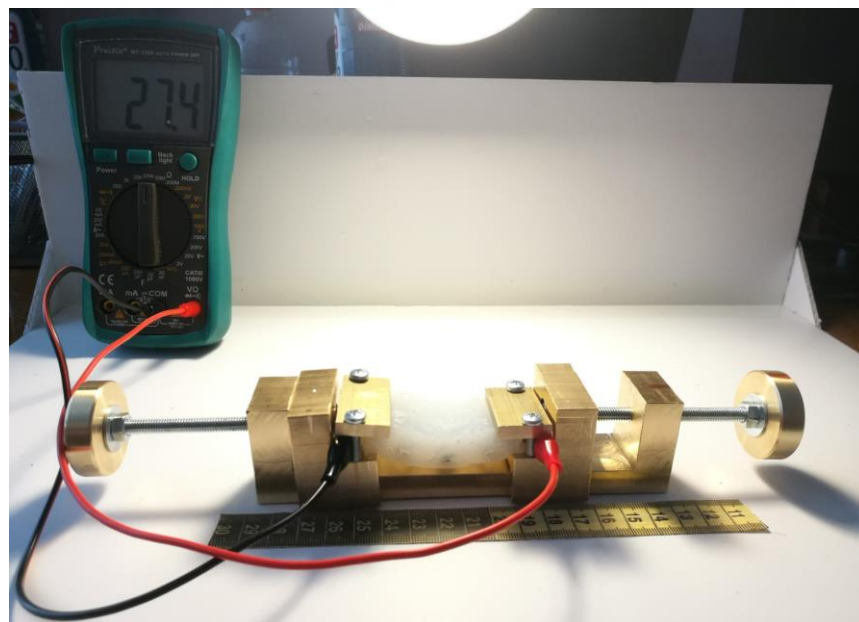
Figure 3.11: Measurement Moment from Tensile Test on All Elements View.

CHAPTER IV

RESULTS & DISCUSSION

4.1 TEST RESULTS

Test results were interpreted in two parts which are tensile test results and bending test results. Results were presented in graphic form and tables of results were added to the appendix part. Trendlines were created on 3rd order polynomial all of the results. 3rd order was selected since to the variable number on the resistance formula. The formula contains area and length as a variable. The area is 2nd order variable and length is 1st order variable, therefore, trendlines were selected as 3rd order polynomial.

Bending test results were examined by analyzing bending angle versus resistance change. Same shapes groups like straight lines and honeycombs were examined in the same graphs and the remaining ones were examined separately. Comments on results were made under the related graphs. For the graphics of the same shaped parts, thicknesses were indicated in the legend on the corner of the graphs.

Slope and resistance formulas are used to compare results with each other and make generalizations. Slope data was given under the related graph. The resistance formula was given as Eq. (4.1) below.

4.1.1 Bending Test Results

The examining process starts with honeycomb profiles. Honeycomb profiles were produced at 0.9 mm, 1.2 mm, and 1.5 mm thicknesses. The same force was applied to the test specimens on different test setups. Gathered data was combined on the graph that can be shown in Figure 4.1.
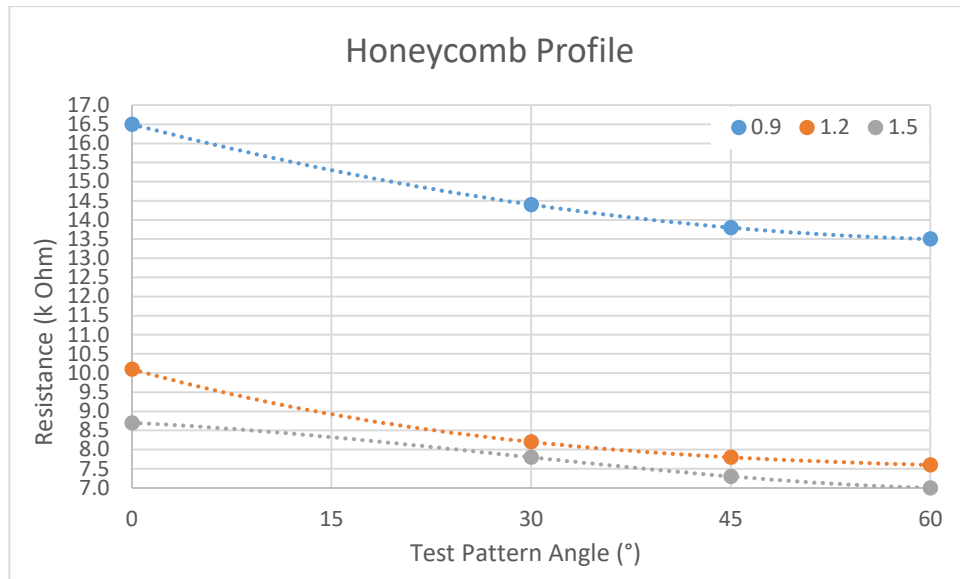
Figure 4.1: Bending Test Results Graph for Honeycomb Profiles.

Table 4.1: Slopes of Honeycomb Profile Trendlines

Thickness	Slope
0.9 mm	-0.05
1.2 mm	-0.04
1.5 mm	-0.03

Resistance decrease with the increasing angle for all honeycomb profile specimens. This can be interpreted as the bending angle being inversely proportional to resistance for honeycomb-shaped profiles. The slope of trendlines is found in Table 4.1. When the slope table was taken into consideration, the effect of thickness over the resistance change can be seen as that increasing thickness caused the decreasing resistance sensitivity. Thickness has a direct proportion over the resistance for honeycomb-shaped profiles.

Straight-line profiles were another trinity group of test specimens. The profiles were produced on 0.4 mm, 0.7 mm and 1.0 mm thicknesses. The same force was applied to the test specimens on different test setups. The gathered data was combined on the graph that can be shown in Figure 4.2.
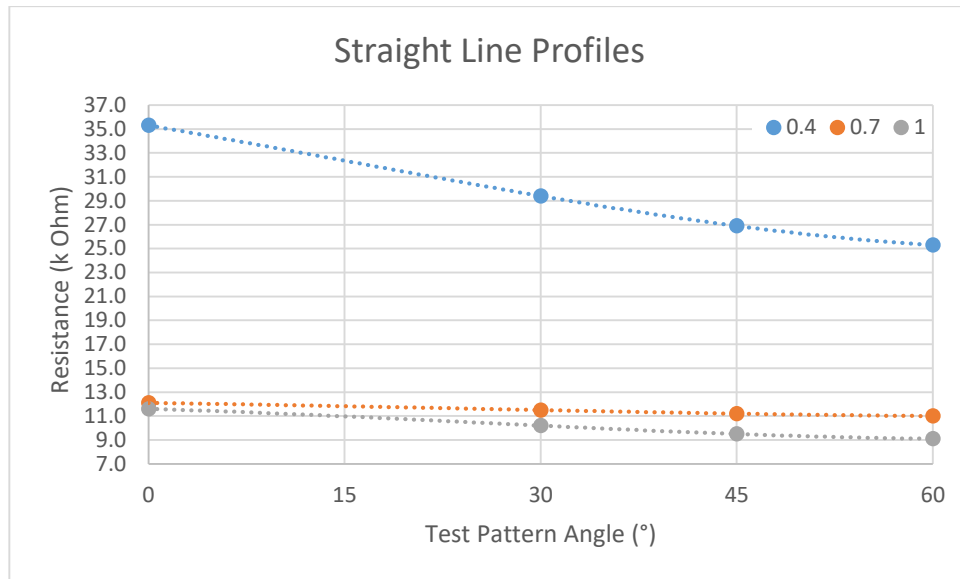
Figure 4.2: Bending Test Results Graph for Straight Line Profiles.

Table 4.2: Slopes of Honeycomb Profile Trendlines

Thickness	Slope
0.4 mm	-0.17
0.7 mm	-0.02
1.0 mm	-0.04

With the increasing angle, resistance for all straight-line profile specimens decreases. In that case, it can be understood that bending angle is inversely proportional to resistance for straight-line profiles. Table 4.2 contains the slope of trendlines. The influence of thickness over resistance change may be recognized when the slope table is taken into account. Increasing thickness results in a decrease in resistance sensitivity. For straight-line-shaped profiles, thickness is directly proportional to resistance.

Rectangular profiles were the first of single-thickness produced test specimens. The profile was produced on 1.0 mm thickness. The same force was applied to the test specimen as to other specimens. Results were presented on the graph that can be shown in Figure 4.3.
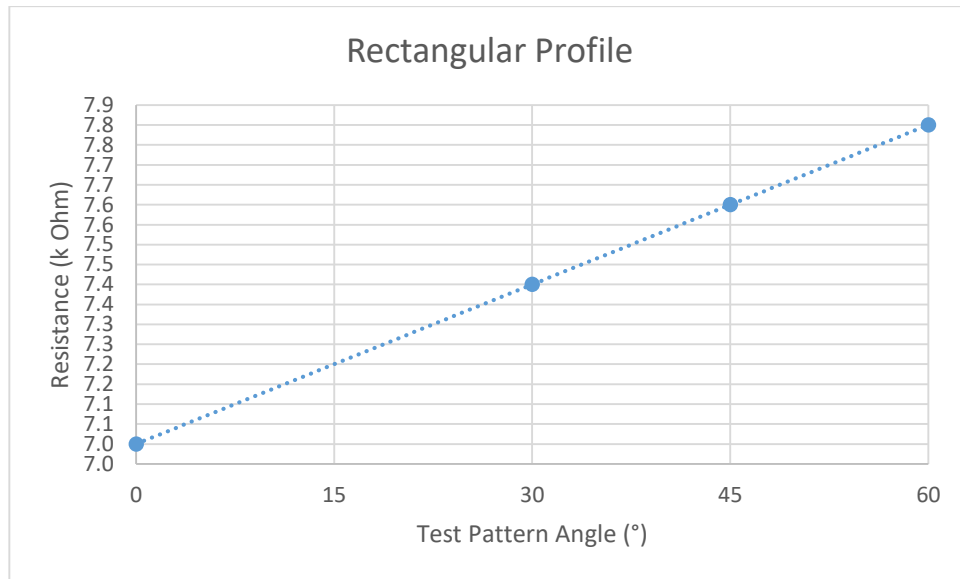
Figure 4.3: Bending Test Results Graph for Rectangular Profile.

Due to using a test specimen with a single thickness, the slope and thickness effect could not be examined. Bending angle has direct proportion with resistance on rectangular profiles. The effect of shapes on the resistance between profiles will be presented at the end of the section.

"Z" shaped profiles were the part of the single-thickness produced test specimens group. The profile thickness was set as 1.0 mm. The same force was applied to the test specimen as to other specimens. Results were presented on the graph that can be shown in Figure 4.4.
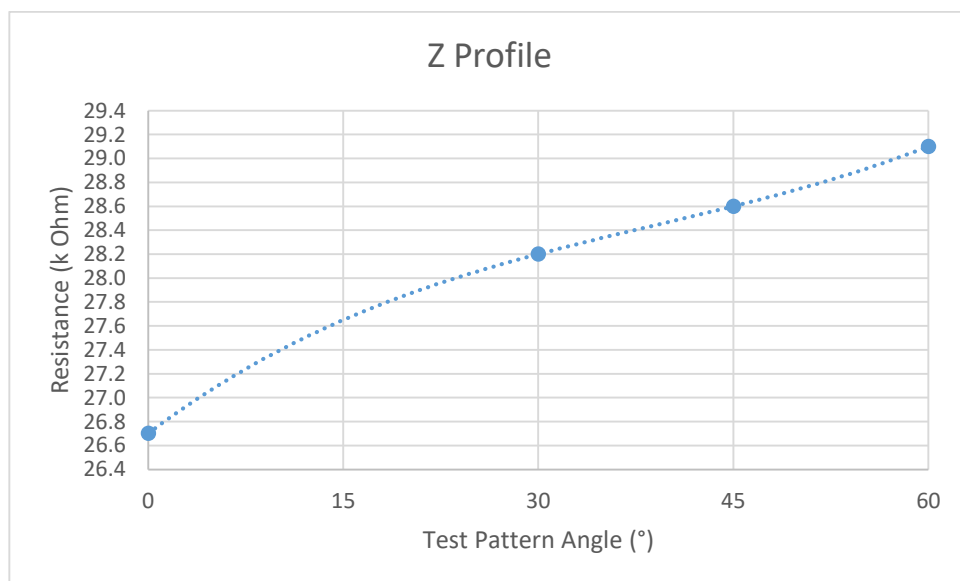
Figure 4.4: Bending Test Results Graph for "Z" Shaped Profile.

The specimen was produced on constant thickness, which means there is no variation in the thickness for the "Z" shaped profile. So, the slope and thickness effect could not be examined. Bending angle and resistance are directly proportional for "Z" shaped profiles.

"S" shaped profiles were the last of single thickness test specimens also produced on 1.0 mm thickness. The same force was applied to the test specimen as to other specimens. Results were presented on the graph that can be shown in Figure 4.5.
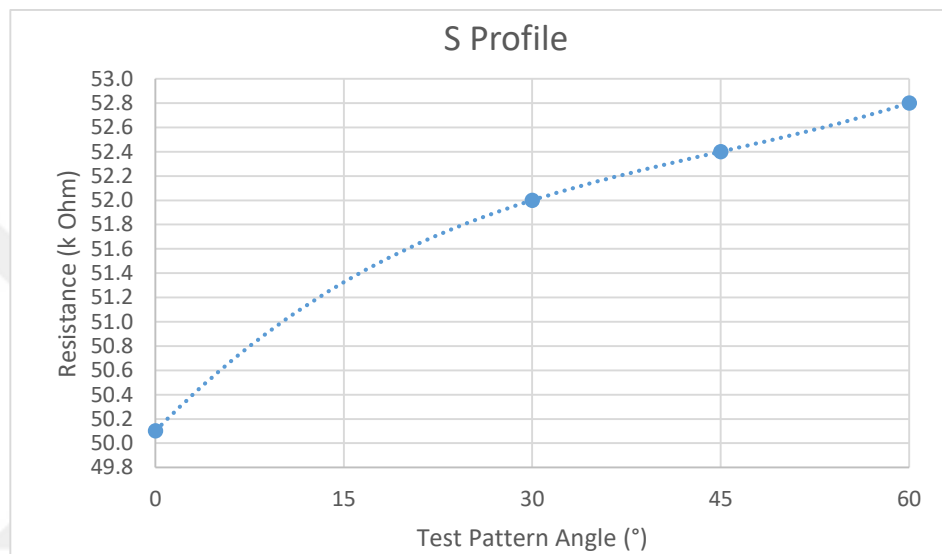
Figure 4.5: Bending Test Results Graph for "S" Shaped Profile.

The profile also has a single thickness; therefore, the slope and thickness effect was not examined. Bending angle has direct proportion with resistance for "s" shaped profiles. The comparison of the effects of the shapes on resistance for all single group profiles will be presented at the end of the section.

4.1.2 Tensile Test Results

The first examination of the tensile test results starts with honeycomb profiles. Thicknesses for honeycomb profiles were set at 0.9 mm, 1.2 mm, and 1.5 mm. Force was kept constant on different test specimens on different test setups by pulling them to the same length. Obtained data were combined on the graph shown in Figure 4.6.
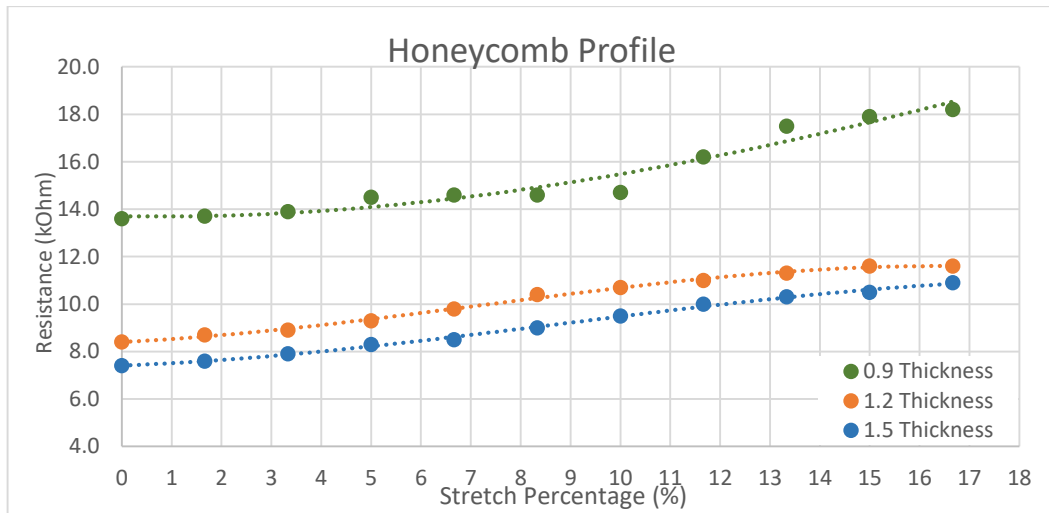
Figure 4.6: Tensile Test Results Graph for Honeycomb Profiles.

Table 4.3: Slopes of Honeycomb Profile Trendlines

Thickness	Slope
0.9 mm	-0.05
1.2 mm	-0.04
1.5 mm	-0.03

Resistance increases with the increasing stretch percentage for all honeycomb profile specimens. This can be interpreted as the stretch percentage is directly proportional to resistance for honeycomb-shaped profiles. The slope of trendlines is found in Table 4.3. The effect of thickness over the resistance change can be seen as that increasing thickness caused the increasing resistance sensitivity when the slope table was considered. Thickness has a direct proportion over the resistance for honeycomb-shaped profiles.
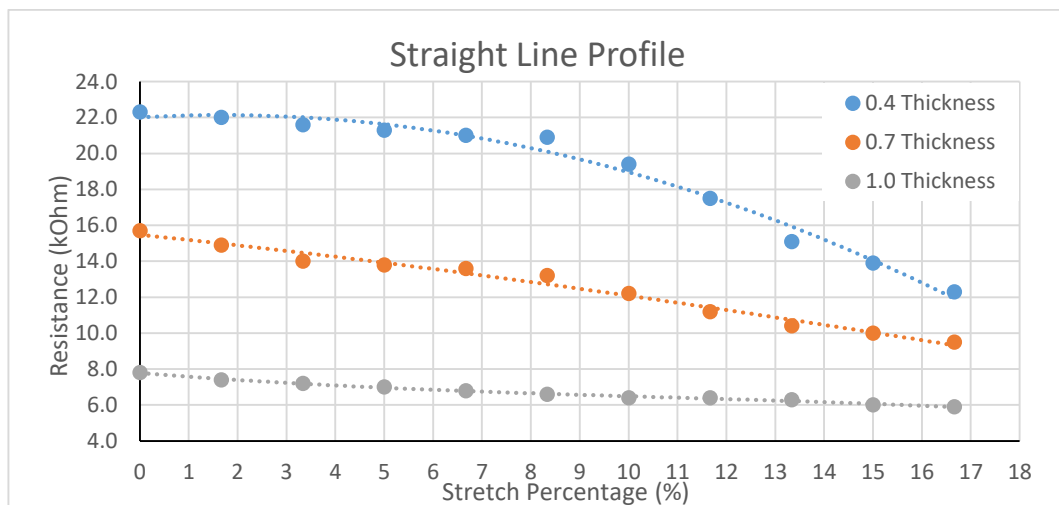
Figure 4.7: Tensile Test Results Graph for Straight Line Profiles.

Table 4.4: Slopes of Honeycomb Profile Trendlines

Thickness	Slope
0.9 mm	-0.05
1.2 mm	-0.04
1.5 mm	-0.03

Test results for straight line profiles were given as Figure 4.7. Resistance acts inversely proportional to stretch percentage on the straight line profiles. The increasing stretch percentage decreases the resistance. Besides, thickness has an inversely proportional relationship with the resistance. Thicker parts show less resistance than the thinner ones. Results are clearly understood by analyzing the slope table which is given in Table 4.4.
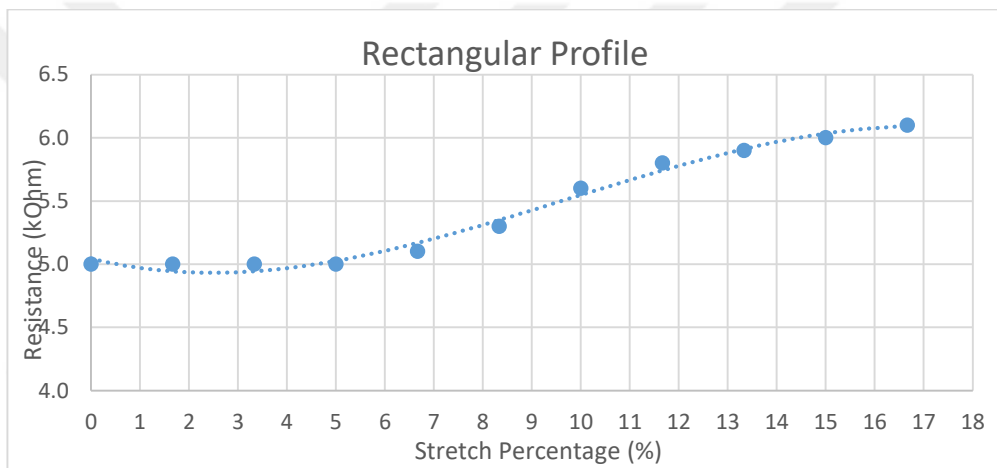
Figure 4.8: Tensile Test Results Graph for Rectangular Profile.
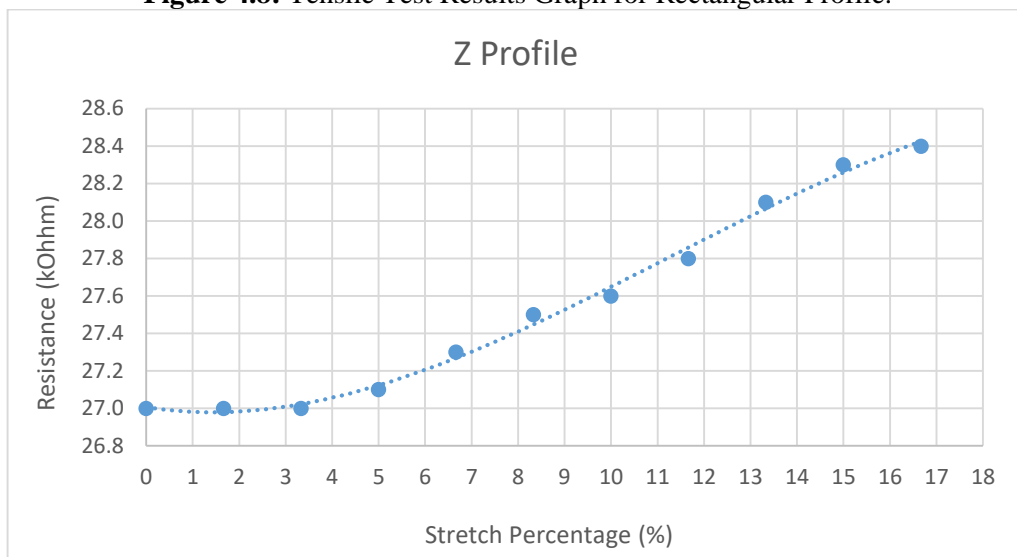
Figure 4.9: Tensile Test Results Graph for "Z" Shaped Profile.
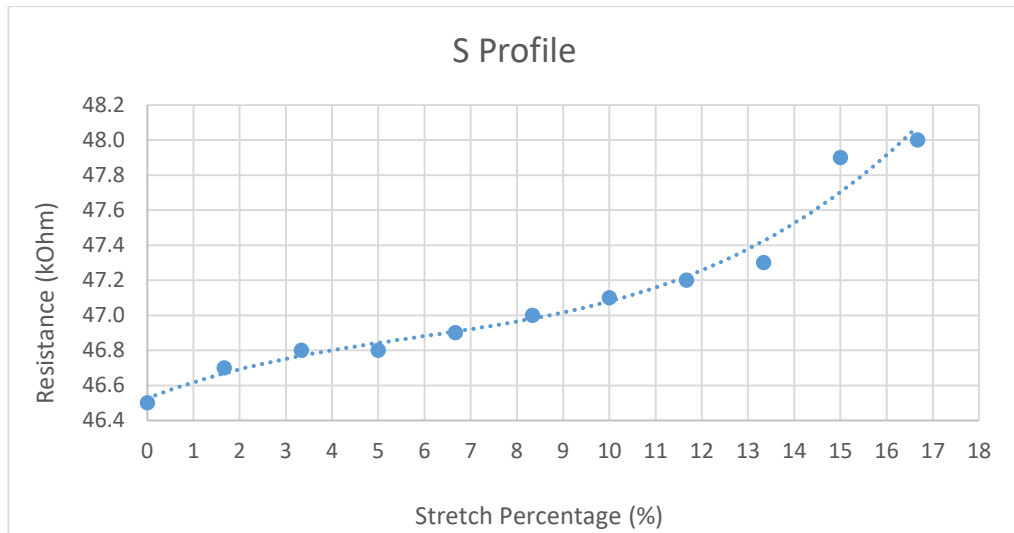
Figure 4.10: Tensile Test Results Graph for "S" Shaped Profile.

The Stretch percentage versus resistance relationship can be found as directly proportional for single thickness models. Test results graphs for models were given as Figure 4.8, Figure 4.9 and Figure 4.10. Since models were planned and produced on a single thickness value, the effect of thickness on resistance change could not be examined for these models.

$$\rho = \frac{(R \; x \; A)}{L} \tag{4.1}$$

Thickness found as inversely proportional to resistance. The implication about thickness can be attributed to the resistivity formula. The formula says resistivity equals area times resistance divided by length. Resistivity is constant for every material and is accepted as a property of the material. Resistivity forms the left side of the equation, so the left side of the equation is constant. This means the right side of the formula should be constant too. For holding the right side of the equation constant numerator part should be constant too. Since increasing thickness increases the area value, resistance should decrease. This mathematical expression clarifies the thickness and resistance relationship.

On the other hand, if the results of stretch percentage versus resistance change are examined, and when the change in length is considered, it can be seen that resistance increase with increasing stretch percentage except for straight line profiles. Again from the resistivity formula, it can be calculated that the right side of the equation decreases due to increasing length under tensile force. Also, thickness decreases to provide the conversation of volume. As a result of these changes,

resistance increases to provide the constancy of the right side of the equation. That situation doesn't work for straight-line profiles due to their large length change. This hypothesis could be examined in future studies.

Bending test results is the most interesting data of the whole experiment. While straight-line profiles and honeycomb profiles have an inverse relationship with bending angle, the remaining profiles show a direct relationship. That could be understood as the resistance of honeycomb and straight-line profiles decreasing with the increasing bending angle, while the resistance of "S" shaped, "Z" shaped, and rectangular-shaped profiles increase with the increasing bending angle. This phenomenon can be explained by the cross-sectional area change of test specimens. While the ratio of area divided by length ($\frac{A}{L}$) for "S," "Z," and rectangular shapes decreases, the same ratio increase for honeycomb and straight-line shapes because of their inner structural differences. Moreover, resistance decreases with the increasing thickness. This inverse ratio could be associated with the increment in the area due to increased thickness. The increasing area also increases the numerator part of the fraction, so resistance decreases to balance the equation.

The final and most important implication is the comparison of different shapes. When the shapes were examined separately for both of the experiments, honeycomb profiles became prominent with the linearity of the graph. The most linear results were obtained on honeycomb profiles. Linearity is the key point in producing sensitive and properly working sensors; thus honeycomb profile was selected and suggested as the best sensor shape for electrically conductive soft robotic elements.

4.2 DISCUSSION

The study made generalizations from the specific to the general from obtained experimental data. When the gathered data was compared with the study of Feng [39], it can be seen that resistance is found to be directly proportional to the bending angle, and result graphs look almost similar to each other according to the linearity and shapes. The results of Feng can be interpreted as there is a direct proportion between the bending angle and the resistance, looking at the results he found by examining the voltage output of the bending sensor. The relationship between resistance and bending angle was found as the same as the thesis work of Feng in this study. Besides, the relationship between thickness and resistance is found as in the same as the article of

Flowers et al. [40]. The scientists found the thickness resistance relationship as inversely proportional. When the graphs provided by the study were examined, it can be seen that the resistance versus length divided by area graph was given. The graph contains three different materials with various thicknesses. Length over area ratio decreases with increasing thickness. The graph represents that resistance decreases with the decreasing length over area ratio. Evaluating all results and this relationship proves that resistance decreases with increasing thickness for all materials as this thesis comments. Those generalizations could answer where the researchers should start and where they should look.

In addition, the output of the study could be used for producing new soft sensor types, which can lead the way for future technologies. Moreover, required technologies like prosthetic limbs could be developed faster with learned information.

Repetition of the experiment with different combinations can verify the experiment and put forward new conflicts to solve and be the starting point of new research. While holding one variable constant like shape, material, or infill ratio, changing others one by one could reveal tens of combinations for future work.

Insulation quality and insulation method should be enhanced in future work. Plastic insulator application or more plastic part usage on test setups could be the key to high-quality insulation.

The observer count could be increased for obtaining more accurate results even artificial intelligence could be included for gathering high-quality data. Digital multimeter quality could be changed for reading more precise results by increasing decimal numbers.

CHAPTER V

CONCLUSION

Unique shapes with various thickness combinations were examined in two different test setups. When the obtained results were gathered, it was seen that the effect of changes made on the thickness in the same direction for different materials was generally the same. Thickness was found as inversely proportional to resistance which means resistance decreases with the increasing thickness.

Besides, when the tensile test results were examined, elongation was found as directly proportional to resistance for all shapes except for straight-line profiles. So it can be understood that while the stretch percentage increase, resistance also increases.

Moreover, implications were made from bending test results. Thickness is found inversely proportional to resistance. Also, the bending angle was determined as directly proportional with resistance for "S," "Z," and rectangular shapes, but on the other hand, the resistance versus bending angle relationship was determined as inversely proportional for honeycomb and straight-line profiles.

The final implication was made about the shape effect on resistance. Honeycomb profiles were observed as the most linear ones in the graph results. Due to high linearity, honeycomb profiles were selected and recommended as the most suitable shape for 3D printed soft conductive sensors.

REFERENCES

1. Lee J. Y., An J. and Chua C. K. (2017), "Fundamentals and applications of 3D printing for novel materials" *İçinde, Applied Materials Today*, Vol. 7, Ed. M. Pumera, p. 120–133, Elsevier Inc., USA.

2. Vilsteren S. Van (2021), *Designing Magnetic Soft Materials for 4D Printing* (MSc Thesis), Delft University of Technology Faculty of Industrial Design Engineering, Delft.

3. Gul J. Z., Sajid M., Rehman M. M., Siddiqui G. U., Shah I., Kim K. H., Lee J. W. and Choi K. H. (2018), "3D printing for soft robotics–a review" *İçinde, Science and Technology of Advanced Materials,* Vol. 19, Ed. K. Hono, p. 243–262, Taylor & Francis, UK.

4. Eric J. Markvicka (2018), *Robust Soft-Matter Robotic Materials* (MSc Thesis), Carnegie Mellon University Robotics Institute, Pittsburgh.

5. Vignali E., Gasparotti E., Capellini K., Fanni B. M., Landini L., Positano V. and Celi S. (2021), "Modeling biomechanical interaction between soft tissue and soft robotic instruments: importance of constitutive anisotropic hyperelastic formulations" *İçinde, International Journal of Robotics Research*, Vol. 40, Ed. J. M. Hollerbach, p. 224–235, Sage Publishing, California.

6. Majidi C. (2018), "Soft-Matter Engineering for Soft Robotics" *İçinde, Advanced Materials Technologies*, Vol. 4, Ed. Esther L., p. 13, John Wiley & Sons, Ltd, Weinheim.

7. Shimoga K. B. and Goldenberg A. A. (1992), "Soft materials for robotic fingers" *Proceedings -IEEE International Conference on Robotics and Automation,* Vol. 2, p. 1300–1305, Nice, FRANCE

8. Thakar C. M., Parkhe S. S., Jain A., Phasinam K., Murugesan G. and Ventayen R. J. M. (2021), "3d Printing: Basic principles and applications" *İçinde, Materials Today: Proceedings*, Vol. 51, Ed. M. Pumera, p. 842–849, Elsevier Inc., USA.

9. Ngo T. D., Kashani A., Imbalzano G., Nguyen K. T. Q. and Hui D. (2018), "Additive manufacturing (3D printing): A review of materials, methods, applications and challenges" *İçinde, Composites Part B: Engineering,* Vol. 143, Ed. Hao W., p. 172–196, Elsevier Inc., USA.

10. Emon M. O. F., Alkadi F., Philip D. G., Kim D. H., Lee K. C. and Choi J. W. (2019), "Multi-material 3D printing of a soft pressure sensor" *İçinde, Additive Manufacturing,* Vol. 28, Ed. Ryan W., p. 629–638, Elsevier Inc., USA.

11. Saptarshi S. M., and Zhou C. (2019), "Basics of 3D Printing: Engineering Aspects" *İçinde, 3D Printing in Orthopaedic Surgery,* Ed. Matthew D. and Felasfa M. W., p. 17-30, Elsevier Inc., USA ; http://dx.doi.org/10.1016/B978-0-323-58118-9.00002-6.

12. Sachyani K. E., Kamyshny A., Totaro M., Beccai L., and Magdassi S. (2021), "3D Printing Materials for Soft Robotics" *İçinde, Advanced Materials.* Vol. 33, Ed. Jos L., p. 1–17, John Wiley & Sons, Ltd, Weinheim.

13. Majidi C. (2014), "Soft Robotics: A Perspective - Current Trends and Prospects for the Future" *İçinde, Soft Robotics (SoRo),* Vol. 1, Ed. Barry A. T., p. 5–11, Mary Ann Liebert, Inc., USA.

14. Appiah C., Arndt C., Siemsen K., Heitmann A., Staubitz A., and Selhuber-Unkel C. (2019), "Living Materials Herald a New Era in Soft Robotics"*İçinde, Advanced Materials*, Vol. 31, Ed. Jos L., John Wiley & Sons, Ltd, Weinheim. doi:10.1002/adma.201807747.

15. Rus D. and Tolley M. T. (2015), "Design, fabrication and control of soft robots" *İçinde, Nature,* Vol. 521, Ed. John M., p. 467–475, Nature Research, UK.

16. Selvi Ö., Telli İ., Totuk O. H. and Mıstıkoğlu S. (2019), " 3D Printing Soft Robots Using Low-Cost Consumer 3D Printers"*4 th International Congress on 3D Printing (Additive Manufacturing) Technologies and Digital Industry*, Ed. K. Çetinkaya, B. Duman, K. Özsoy, K. Kayaalp, O. Oral, M. Aydın, Eds. p., 1016–1021, Antalya.

17. Wallin T. J., Pikul J. and Shepherd R. F. (2018), "3D printing of soft robotic systems" *İçinde, Nature,* Vol. 3, Ed. John M., p. 84–100, Nature Research, UK.

18. Yap Y. L., Sing S. L. and Yeong W. Y. (2020), "A review of 3D printing processes and materials for soft robotics" *İçinde, Rapid Prototyping Journal*,

Vol. 26, Ed. Ian G., p. 1345–1361, Emerald Publishing Limited, UK.

19. Somm L., Hahn D., Kumar N. and Coros, S. (2019), "Expanding Foam as the Material for Fabrication, Prototyping and Experimental Assessment of Low-Cost Soft Robots With Embedded Sensing" *İçinde, IEEE Robotics and Automation Letters*, Vol. 4, Ed. Tamim A., p. 761–768, IEEE Inc., USA

20. Khan S. F., Zakaria H., Chong Y. L., Saad M. A. M. and Basaruddin K. (2018), "Effect of infill on tensile and flexural strength of 3D printed PLA parts" *İçinde, IOP Conference Series: Materials Science and Engineering,* Vol. 429, Ed. Matin L., IOP Publishing Ltd., UK., doi:10.1088/1757-899X/429/1/012101.

21. Fernandez-Vicente M., Calle W., Ferrandiz S. and Conejero A. (2016), "Effect of Infill Parameters on Tensile Mechanical Behavior in Desktop 3D Printing" *İçinde, 3D Printing and Additive Manufacturing*, Vol. 3, Ed. Skylar T., p. 183–192, Mary Ann Liebert, Inc., USA.

22. Selvi Ö., Totuk O. H., Mistikoğlu S. and Arslan, O. (2021), "Strengthening Effect of Flooding in 3D Printed Porous Soft Robotics Scaffolds" *İçinde, International Journal of 3D Printing Technologies and Digital Industry*, Vol. 5, Ed. Kerim Ç., p. 293–301, Kerim Çetinkaya, Turkey.

23. Polygerinos P., Correll N., Morin S. A., Mosadegh B., Onal C. D., Petersen K., Cianchetti M., Tolley M. T. and Shepherd R. F. (2017), "Soft Robotics: Review of Fluid-Driven Intrinsically Soft Devices; Manufacturing, Sensing, Control, and Applications in Human-Robot Interaction" *İçinde, Advanced Engineering Materials*, Vol. 19, Ed. Sandra K., p. 1700016, John Wiley & Sons, Ltd, Weinheim.

24. Gorissen B., Reynaerts D., Konishi S., Yoshida K., Kim J.-W. and De Volder M. (2017), "Elastic Inflatable Actuators for Soft Robotic Applications" *İçinde, Advanced Materials*, Vol. 29, Ed. Jos L., p. 1604977, John Wiley & Sons, Ltd, Weinheim.

25. Runciman M., Darzi A. and Mylonas G. P. (2019), "Soft Robotics in Minimally Invasive Surgery" *İçinde, Soft Robotics (SoRo),* Vol. 6, Ed. Barry A. T., p. 423–443, Mary Ann Liebert, Inc., USA.

26. Totuk O. H., Başak H. (2017), " Biyomimetik Eklemeli İmalat: 4B Basım"*2. International Symposium on Industrial Design and Engineering-ISIDE,*

Nevşehir.

27. Cho K. J., Koh J. S., Kim S., Chu W. S., Hong Y. and Ahn S. H. (2009), "Review of manufacturing processes for soft biomimetic robots" *İçinde, International Journal of Precision Engineering and Manufacturing*, Vol. 10, Ed. Byung-Kwon M., p. 171–181, Springer Nature, Switzerland.

28. Coyle S., Majidi C., LeDuc P. and Hsia K. J. (2018), "Bio-inspired soft robotics: Material selection, actuation, and design" *İçinde, Extreme Mechanics Letters*, Vol. 22, Ed. John A. R.,p. 51–59, Elsevier Inc., USA.

29. Margheri L., Laschi C. and Mazzolai B. (2012), "Soft robotic arm inspired by the octopus: I. from biological functions to artificial requirements" *İçinde, Bioinspiration and Biomimetics,* Vol. 7, Ed. Cecilia L., IOP Publishing Ltd., UK., doi:10.1088/1748-3182/7/2/025004.

30. Lo C. Y., Zhao Y., Kim C., Alsaid Y., Khodambashi R., Peet M., Fisher R., Marvi H., Berman S., Aukes D. and He X. (2021), "Highly stretchable self-sensing actuator based on conductive photothermally-responsive hydrogel" *İçinde,Materials Today*, Vol. 50, Ed. Jun L., p. 35–43, Elsevier Inc., USA.

31. Stoyanov H., Kollosche M., Risse S., Waché R. and Kofod G. (2013), "Soft conductive elastomer materials for stretchable electronics and voltage controlled artificial muscles" *İçinde, Advanced Materials Technologies*, Vol. 25, Ed. Esther L., p. 578-583, John Wiley & Sons, Ltd, Weinheim.

32. Tang L., Wu S., Qu J., Gong L. and Tang J. (2020), "A review of conductive hydrogel used in flexible strain sensor" *İçinde, Materials*, Vol. 13, Ed. Yulia Z., p. 1–17, MDPI, Basel.

33. Kwok S. W., Goh K. H. H., Tan Z. D., Tan S. T. M., Tjiu W. W., Soh J. Y., Ng Z. J. G., Chan Y. Z., Hui H. K. and Goh K. E. J. (2017), "Electrically conductive filament for 3D-printed circuits and sensors" *İçinde, Applied Materials Today*, Vol. 9, Ed. M. Pumera, p. 167–175, Elsevier Inc., USA.

34. Hart A. M. (2018), *Positional Estimation Of Soft Actuators Through Embedded Sensing* (MSc Thesis), Georgia Institute of Technology Faculty of George W. Woodruff School of Mechanical Engineering, Atlanta.

35. Case J. C., White E. L. and Kramer R. K. (2015), "Soft material characterization for robotic applications" *İçinde, Soft Robotics (SoRo),* Vol. 2, Ed. Barry A. T., p. 80-87, Mary Ann Liebert, Inc., USA.

36. Hemleben S. (2017), *Modeling a Spectrum of 3D Printed Materials for Soft Robots* (MSc Thesis), Oregon State University School of Mechanical Industrial and Manufacturing Engineering, Oregon.

37. Dong S. K. (2016), *Hydrostatic 3D-Printing for Soft Material Structures Using Low One-Photon Polymerization* (MSc Thesis), Texas A&M University Office of Graduate and Professional Studies, Texas.

38. Tiley A. R. and Dreyfuss H. (2002), *The Measure of man and woman: human factors in design,* John Wiley & Sons, Ltd, New York.

39. Ni F. (2016), *Experimental Characterization and Design of Soft Robotics* (MSc Thesis), The Hong Kong University of Science and Technology Department of Mechanical and Aerospace Engineering, Hong Kong.

40. Flowers P. F., Reyes C., Ye S., Kim M. J. and Wiley B. J. (2017), "3D printing electronic components and circuits with conductive thermoplastic filament" *İçinde, Additive Manufacturing,* Vol. 18, Ed. Ryan W., p. 156-163, Elsevier Inc., USA.

APPENDICES

OTHER PROFILES					
Z Profile		S Profile		Rectangular Profile	
Angle	*Resistance*	*Angle*	*Resistance*	*Angle*	*Resistance*
0 °	26.7 *k Ohm*	0 °	50.1 *k Ohm*	0 °	7.0 *k Ohm*
30 °	28.2 *k Ohm*	30 °	52.0 *k Ohm*	30 °	7.4 *k Ohm*
45 °	28.6 *k Ohm*	45 °	52.4 *k Ohm*	45 °	7.6 *k Ohm*
60 °	29.1 *k Ohm*	60 °	52.8 *k Ohm*	60 °	7.8 *k Ohm*

STRAIGHT LINE PROFILES					
0.4 mm Thickness		0.7 mm Thickness		1.0 mm Thickness	
Angle	*Resistance*	*Angle*	*Resistance*	*Angle*	*Resistance*
0 °	35.3 *k Ohm*	0 °	12.1 *k Ohm*	0 °	11.6 *k Ohm*
30 °	29.4 *k Ohm*	30 °	11.5 *k Ohm*	30 °	10.2 *k Ohm*
45 °	26.9 *k Ohm*	45 °	11.2 *k Ohm*	45 °	9.5 *k Ohm*
60 °	25.3 *k Ohm*	60 °	11.0 *k Ohm*	60 °	9.1 *k Ohm*

HONEYCOMB PROFILES					
0.9 mm Thickness		1.2 mm Thickness		1.5 mm Thickness	
Angle	*Resistance*	*Angle*	*Resistance*	*Angle*	*Resistance*
0 °	16.5 *k Ohm*	0 °	10.1 *k Ohm*	0 °	8.7 *k Ohm*
30 °	14.4 *k Ohm*	30 °	8.2 *k Ohm*	30 °	7.8 *k Ohm*
45 °	13.8 *k Ohm*	45 °	7.8 *k Ohm*	45 °	7.3 *k Ohm*
60 °	13.5 *k Ohm*	60 °	7.6 *k Ohm*	60 °	7.0 *k Ohm*

OTHER PROFILES								
Z Profile			S Profile			Rectangular Profile		
Length	*Strech*	*Resistance*	*Length*	*Strech*	*Resistance*	*Length*	*Strech*	*Resistance*
60 mm	0 mm	27.0 *k Ohm*	60 mm	0 mm	46.5 *k Ohm*	60 mm	0 mm	5.0 *k Ohm*
61 mm	1 mm	27.0 *k Ohm*	61 mm	1 mm	46.7 *k Ohm*	61 mm	1 mm	5.0 *k Ohm*
62 mm	2 mm	27.0 *k Ohm*	62 mm	2 mm	46.8 *k Ohm*	62 mm	2 mm	5.0 *k Ohm*
63 mm	3 mm	27.1 *k Ohm*	63 mm	3 mm	46.8 *k Ohm*	63 mm	3 mm	5.0 *k Ohm*
64 mm	4 mm	27.3 *k Ohm*	64 mm	4 mm	46.9 *k Ohm*	64 mm	4 mm	5.1 *k Ohm*
65 mm	5 mm	27.5 *k Ohm*	65 mm	5 mm	47.0 *k Ohm*	65 mm	5 mm	5.3 *k Ohm*
66 mm	6 mm	27.6 *k Ohm*	66 mm	6 mm	47.1 *k Ohm*	66 mm	6 mm	5.6 *k Ohm*
67 mm	7 mm	27.8 *k Ohm*	67 mm	7 mm	47.2 *k Ohm*	67 mm	7 mm	5.8 *k Ohm*
68 mm	8 mm	28.1 *k Ohm*	68 mm	8 mm	47.3 *k Ohm*	68 mm	8 mm	5.9 *k Ohm*
69 mm	9 mm	28.3 *k Ohm*	69 mm	9 mm	47.9 *k Ohm*	69 mm	9 mm	6.0 *k Ohm*
70 mm	10 mm	28.4 *k Ohm*	70 mm	10 mm	48.0 *k Ohm*	70 mm	10 mm	6.1 *k Ohm*

STRAIGHT LINE PROFILES								
0.4 mm Thickness			0.7 mm Thickness			1.0 mm Thickness		
Length	*Strech*	*Resistance*	*Length*	*Strech*	*Resistance*	*Length*	*Strech*	*Resistance*
60 mm	0 mm	22.3 *k Ohm*	60 mm	0 mm	15.7 *k Ohm*	60 mm	0 mm	7.8 *k Ohm*
61 mm	1 mm	22.0 *k Ohm*	61 mm	1 mm	14.9 *k Ohm*	61 mm	1 mm	7.4 *k Ohm*
62 mm	2 mm	21.6 *k Ohm*	62 mm	2 mm	14.0 *k Ohm*	62 mm	2 mm	7.2 *k Ohm*
63 mm	3 mm	21.3 *k Ohm*	63 mm	3 mm	13.8 *k Ohm*	63 mm	3 mm	7.0 *k Ohm*
64 mm	4 mm	21.0 *k Ohm*	64 mm	4 mm	13.6 *k Ohm*	64 mm	4 mm	6.8 *k Ohm*
65 mm	5 mm	20.9 *k Ohm*	65 mm	5 mm	13.2 *k Ohm*	65 mm	5 mm	6.6 *k Ohm*
66 mm	6 mm	19.4 *k Ohm*	66 mm	6 mm	12.2 *k Ohm*	66 mm	6 mm	6.4 *k Ohm*
67 mm	7 mm	17.5 *k Ohm*	67 mm	7 mm	11.2 *k Ohm*	67 mm	7 mm	6.4 *k Ohm*
68 mm	8 mm	15.1 *k Ohm*	68 mm	8 mm	10.4 *k Ohm*	68 mm	8 mm	6.3 *k Ohm*
69 mm	9 mm	13.9 *k Ohm*	69 mm	9 mm	10.0 *k Ohm*	69 mm	9 mm	6.0 *k Ohm*
70 mm	10 mm	12.3 *k Ohm*	70 mm	10 mm	9.5 *k Ohm*	70 mm	10 mm	5.9 *k Ohm*

HONEYCOMB PROFILES								
0.9 mm Thickness			1.2 mm Thickness			1.5 mm Thickness		
Length	*Strech*	*Resistance*	*Length*	*Strech*	*Resistance*	*Length*	*Strech*	*Resistance*
60 mm	0 mm	13.6 *k Ohm*	60 mm	0 mm	8.4 *k Ohm*	60 mm	0 mm	7.4 *k Ohm*
61 mm	1 mm	13.7 *k Ohm*	61 mm	1 mm	8.7 *k Ohm*	61 mm	1 mm	7.6 *k Ohm*
62 mm	2 mm	13.9 *k Ohm*	62 mm	2 mm	8.9 *k Ohm*	62 mm	2 mm	7.9 *k Ohm*
63 mm	3 mm	14.5 *k Ohm*	63 mm	3 mm	9.3 *k Ohm*	63 mm	3 mm	8.3 *k Ohm*
64 mm	4 mm	14.6 *k Ohm*	64 mm	4 mm	9.8 *k Ohm*	64 mm	4 mm	8.5 *k Ohm*
65 mm	5 mm	14.6 *k Ohm*	65 mm	5 mm	10.4 *k Ohm*	65 mm	5 mm	9.0 *k Ohm*
66 mm	6 mm	14.7 *k Ohm*	66 mm	6 mm	10.7 *k Ohm*	66 mm	6 mm	9.5 *k Ohm*
67 mm	7 mm	16.2 *k Ohm*	67 mm	7 mm	11.0 *k Ohm*	67 mm	7 mm	10.0 *k Ohm*
68 mm	8 mm	17.5 *k Ohm*	68 mm	8 mm	11.3 *k Ohm*	68 mm	8 mm	10.3 *k Ohm*
69 mm	9 mm	17.9 *k Ohm*	69 mm	9 mm	11.6 *k Ohm*	69 mm	9 mm	10.5 *k Ohm*
70 mm	10 mm	18.2 *k Ohm*	70 mm	10 mm	11.6 *k Ohm*	70 mm	10 mm	10.9 *k Ohm*

Figure: Results Table for Both Tests.